Supplemental Information

RBPMS, an RNA-binding protein that mediates cardiomyocyte binucleation and cardiovascular development

Peiheng Gan, Zhaoning Wang, Maria Gabriela Morales, Yu Zhang, Rhonda Bassel-Duby, Ning Liu & Eric N. Olson

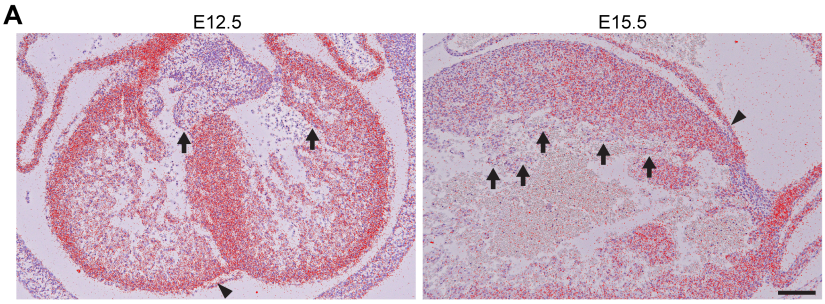

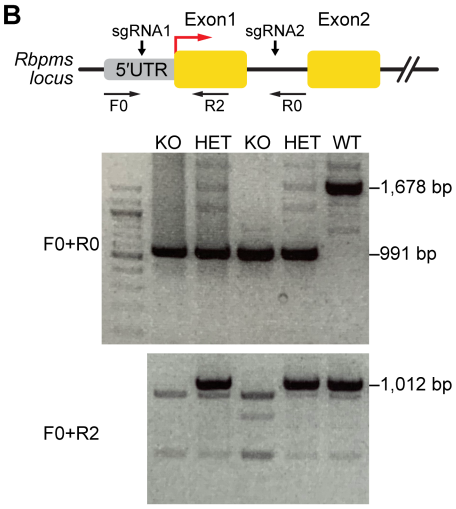

C

Genotype	Expected	Observed	Ratio
WT	30.5	34	0.258
HET	61	63	0.477
KO	30.5	35	0.265
Total	132	132	1

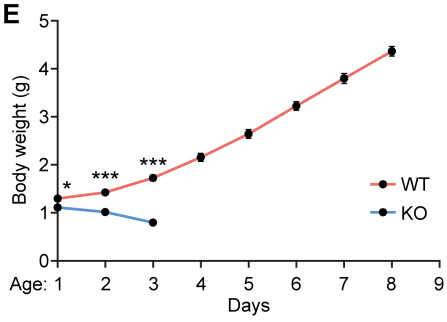

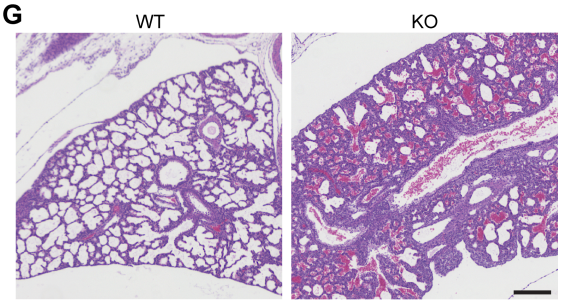

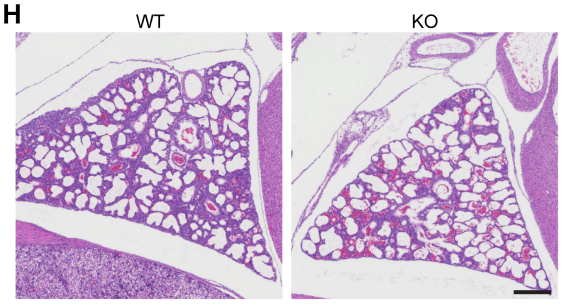

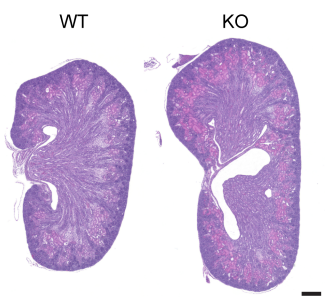

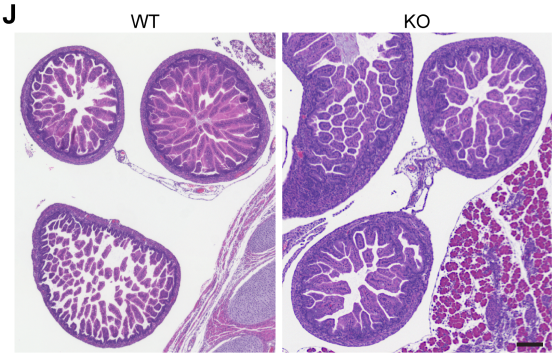

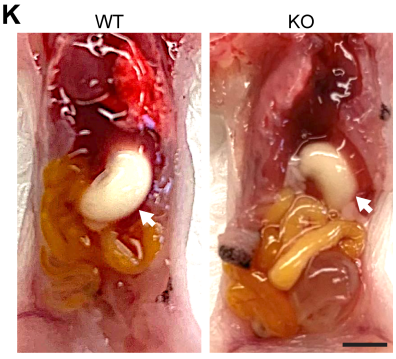

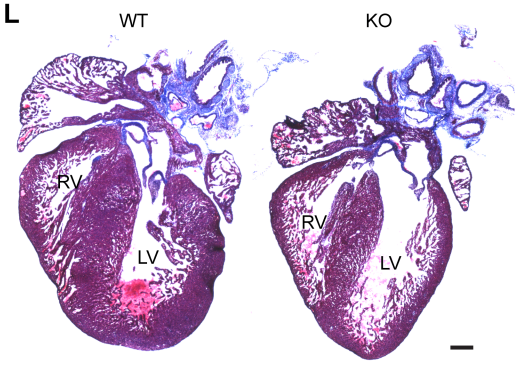

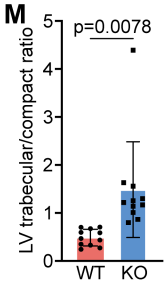

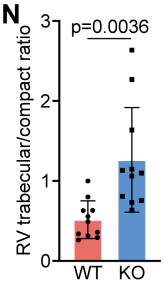

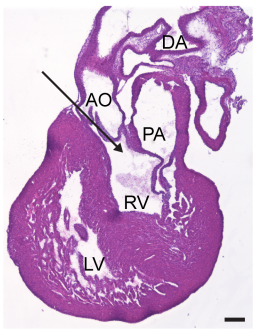

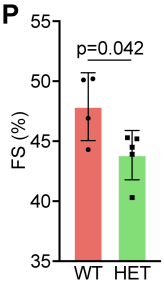

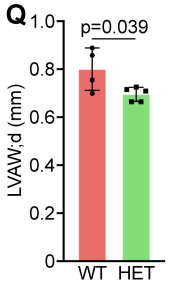

Supplemental Figure 1

Supplemental Figures, Tables and Legends

Figure S1. Phenotypes of *Rbpms* KO mouse, Related to Figure 1.

A. High magnification (10X) images related to Figure 1B, and showing the expression of *Rbpms* mRNA in hearts at the indicated embryonic time points. Black arrows indicate *Rbpms* mRNA expression in endocardium and black arrowheads indicate myocardium. Scale bar: 30 μm. **B.** Gene structure of mouse *Rbpms* and knock-out strategy (Top). Black arrows indicate the locations of sgRNA1 and sgRNA2. Boxes represent exons and untranslated region (UTR). Horizontal black arrows indicate primers for genotyping. Genotyping of *Rbpms* KO mice by PCR (Bottom). Primers F0 and R0 recognize both WT (1,678 bp) and KO (991 bp) alleles. Primers F0 and R2 recognize the WT allele at 1,012 bp. **C.** Table showing the number of mice of indicated genotypes obtained from the *Rbpms* heterozygous intercrosses. The expected mouse number was calculated according to the total number of mice born and based on the expected Mendelian ratio. **D.** Representative image of *Rbpms* WT and KO pups at P1. Scale bar: 5 mm. **E.** Measurements of body weight at different postnatal time points (n = 15 for WT, and 10 for KO. *p<0.05, ***P<0.001). **F.** Lungs from P3 WT and dead KO pups. Scale bar: 200 μm. **G.** H&E-stained sections of representative lungs from P3 WT and dead KO pups. Scale bar: 50 μm. **H.** H&E-stained lung sections of P0 WT and KO pups. Scale bar: 50 μm. **I, J.** H&E-stained sections of representative kidneys and intestines from P1 WT and KO pups. Scale bar: 30 μm. **K.** Autopsy images of P1 WT and KO pups. White arrows point to stomach. Scale bar: 400 μm. **L.** Masson's trichrome-stained coronal sections of P1 WT and KO hearts. LV: left ventricle; RV: right ventricle. Scale bar: 300 μm. **M, N.** Quantification of left ventricular (LV) trabecular zone/compact myocardium thicknesses and right ventricular (RV) trabecular zone/compact myocardium thicknesses of WT and KO mouse hearts at P1 (n = 11 for WT and KO). **O**. H&E-stained sagittal section revealed the double outlet right ventricle (DORV) in P1 KO heart. PA, pulmonary artery; DA: ductus arteriosus; Ao, aorta; LV: left ventricle; RV: right ventricle. Black arrow indicates DORV. Scale bar: 30 μm. **P, Q.** Measurements of fractional shortening (FS%) and LV anterior wall thickness at end cardiac

diastole (LVAW;d) of WT and HET hearts at 4 months of age (n = 4 for WT, and 5 for HET). All data are presented as mean ± SEM.

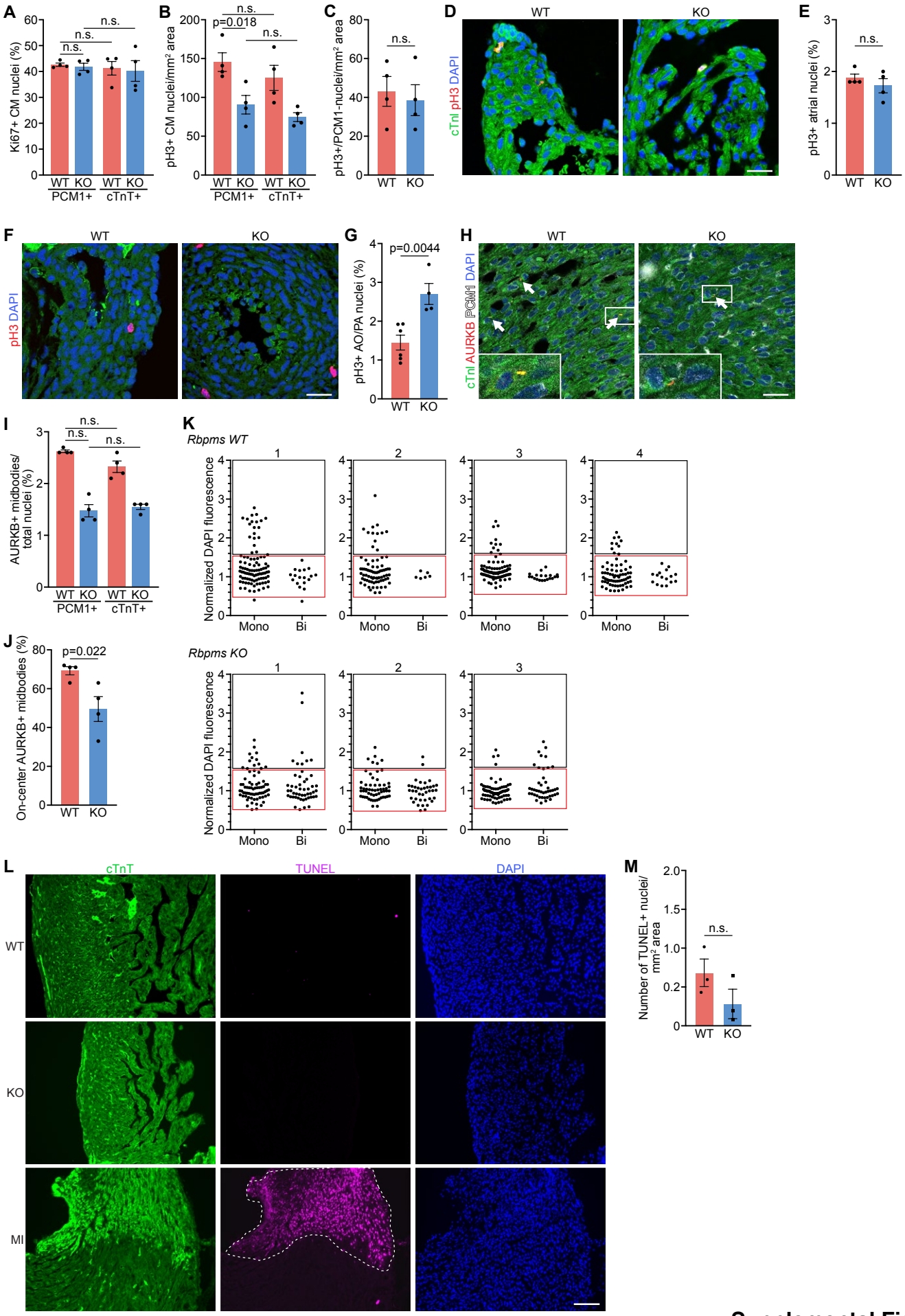

Supplemental Figure 2

Figure S2. Proliferation, ploidy analysis and TUNEL assay in P1 hearts, Related to Figure 2.

A. Quantification of Ki67-positive cardiomyocyte nuclei (PCM1-positive or cTnT-positive) over total nuclei in WT and KO hearts at P1 (n = 4 for WT and KO). n.s., not significant. **B.** Quantification of pH3-positive cardiomyocyte nuclei (PCM1-positive or cTnT-positive) per mm^2 area in WT and KO hearts at P1 (n = 4 for WT and KO). n.s., not significant. **C.** Quantification of pH3-positive, PCM1-negative non-CM nuclei per mm^2 area in WT and KO hearts at P1 (n = 4 for WT and KO). n.s., not significant. **D, E.** Immunofluorescence staining for pH3, cTnI and DAPI of WT and KO heart atria at P1 and quantification of pH3+ atrial CM nuclei over total nuclei. (n = 4 for WT and KO). n.s., not significant. Scale bar: 30 μm. **F, G.** Immunofluorescence staining for pH3 and DAPI in WT and KO heart aorta (at P1 and quantification of number of pH3+ Ao or pulmonary arterial (PA) nuclei over total nuclei. (n = 6 for WT and n=4 for KO). Scale bar: 30 μm. **H, I.** Immunofluorescence staining for aurora B kinase (AURKB), cTnI and DAPI in WT and KO heart myocardium at P1 and quantification of AURKB-positive midbody frequency over total cardiomyocyte nuclei (PCM1-positive or cTnT-positive) (n = 4 for WT and KO). White arrows indicate AURKB-positive midbodies in between nuclei. Scale bar: 30 μm. **J.** Percentage of on-center AURKB-positive midbodies in WT and KO hearts at P1 related to Figure 2H (n = 4 for WT and KO). **K.** Cardiomyocyte ploidy analysis of 4 WT and 3 KO hearts. Each graph represents ventricular cardiomyocytes of one animal. The dots in the red box stand for diploid (2N) nuclei in both mononucleated and binucleated cardiomyocyte populations, and the black box includes hyperploid (>2N) nuclei in both mononucleated and binucleated cardiomyocyte populations. The percentages of 2N and >2N nuclei in each cardiomyocyte population of each heart were calculated based on the graphs, and the data points are used for the graph in Figure 2K. **L.** Immunofluorescence staining for cTnT and TUNEL staining of WT and KO hearts at P1. Adult myocardial infarction (MI) heart section was used as a positive control for TUNEL staining. White

dashed line outlines infarct region on MI heart section. Scale bar: 50 μm. **M.** Quantification of the TUNEL-positive cardiomyocyte nuclei in WT and KO hearts at P1 (n = 3 for WT and KO). n.s., not significant. All data are presented as mean ± SEM.

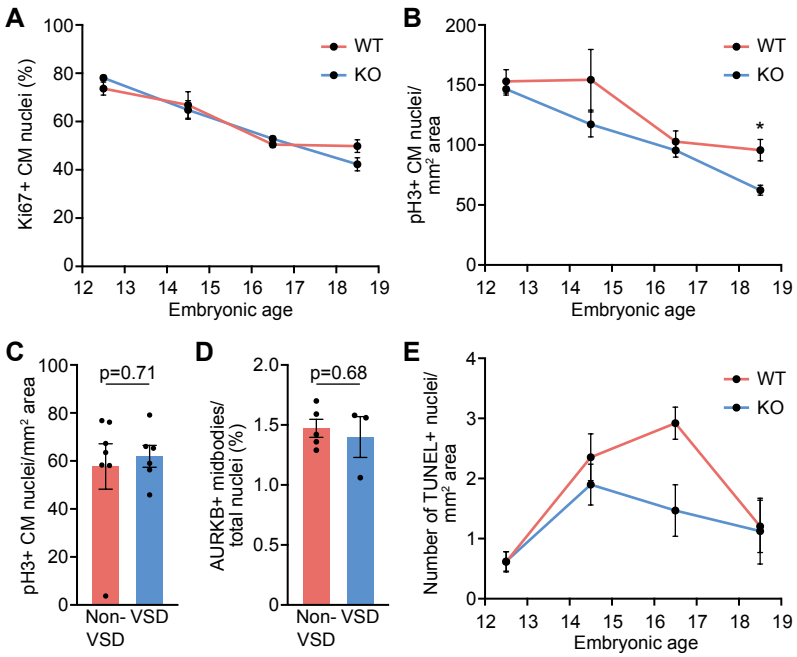

Supplemental Figure 3

Figure S3. Cardiomyocyte proliferation and apoptosis assessment of *Rbpms* KO embryonic hearts, Related to Figure 3.

A. Quantification of percentage of Ki67-positive cardiomyocyte nuclei in embryonic hearts (n = 5-7 for WT and KO at each time point). **B.** Quantification of frequency of pH3-positive cardiomyocyte nuclei in embryonic hearts (n = 5-7 for WT and KO at each time point, *p<0.05). **C, D.** Quantification of frequency of pH3-positive cardiomyocyte nuclei and AURKB-positive midbodies in E18.5 and P1 KO hearts with or without ventricular septal defects (VSDs) (n =5- 7 for non-VSD hearts and n=3-6 for VSD hearts). **E.** Quantification of TUNEL-positive cardiomyocyte nuclei frequency in WT and KO hearts at each developmental time point (n = 3 for WT and KO). All data are presented as mean ± SEM.

A

```
Length: 197
# Identity: 194/197 (98.5%)
# Similarity:195/197 (99.0%)
# Gaps: 1/197 ( 0.5%)
# Score: 1018.0

Human_RBPMS       1 MNGGGKAEKENTPSEANLQEEEVRTLFVSGLPLDIKPRELYLLFRPFKGY    50
                    ||.||||||||||||||||||||||||||||||||||||||||||||||||
Mouse_RBPMS       1 MNNGGKAEKENTPSEANLQEEEVRTLFVSGLPLDIKPRELYLLFRPFKGY    50

Human_RBPMS      51 EGSLIKLTSKQPVGFVSFDSRSEAEAAKNALNGIRFDPEIPQTLRLEFAK   100
                    ||||||||||||||||||||||||||||||||||||||||||||||||||||
Mouse_RBPMS      51 EGSLIKLTSKQPVGFVSFDSRSEAEAAKNALNGIRFDPEIPQTLRLEFAK   100

Human_RBPMS     101 ANTKMAKNKLVGTPNPSTPLPNTVPQFIAREPYELTVPALYPSSPEVWAP   150
                    ||||||||||||||||||||||||||||||||||||||||||||||||||||
Mouse_RBPMS     101 ANTKMAKNKLVGTPNPSTPLPNTVPQFIAREPYELTVPALYPSSPEVWAP   150

Human_RBPMS     151 YPLYPAELAPALPPPAAFTYPASLHAQMRWIPPSEATSQGWKSRQFC      197
                    |||||||||||||||| |||||||||||||:||||||||||||||||
Mouse_RBPMS     151 YPLYPAELAPALPPP-AFTYPASLHAQMRWLPPSEATSQGWKSRQFC      196
```

B

C

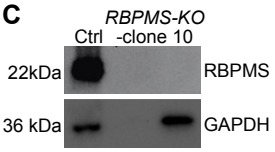

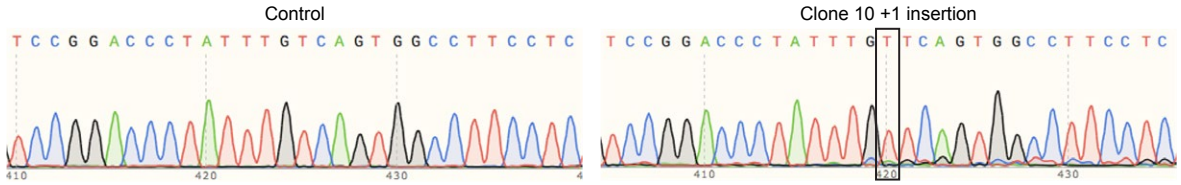

Control-*RBPMS*-ORF:

MNGGGKAEKENTPSEANLQEEEVRTLFVSGLPLDIKPRELYLLFRPFKGYEGSLIKLTSKQPVGFVSFDSRSEAEAAKNALNGIRFDPEIPQTLRLEFAKANTKMAKNKLVGTP
NPSTPLPNTVPQFIAREPYELTVPALYPSSPEVWAPYPLYPAELAPALPPPAAFTYPASLHAQMRWIPPSEATSQGWKSRQFC-

Clone 10-*RBPMS*-ORF:

MNGGGKAEKENTPSEANLQEEEVRTLFVQRSASGHQAPRAVPALQTIQGL-RFSHKAHI-TARRLCQF-QSLRSRGRKERFERHPLRS-NPANATTRVC-GKHEDGQEQTRRDS
KPQYSSAQHCTSVHCQGAI-AHSTCTLPQ-P-SLGPVPSVPSGVSACSSSSCRFHLPRFTACPDALDPSLRGHFPGLEVPAVLL

D

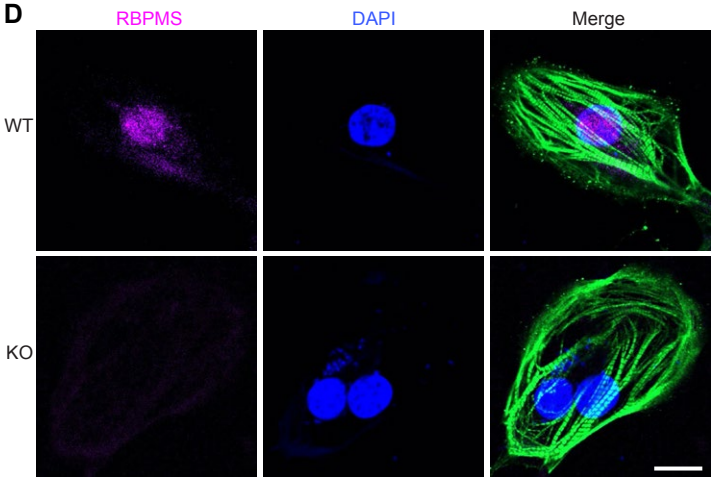

E

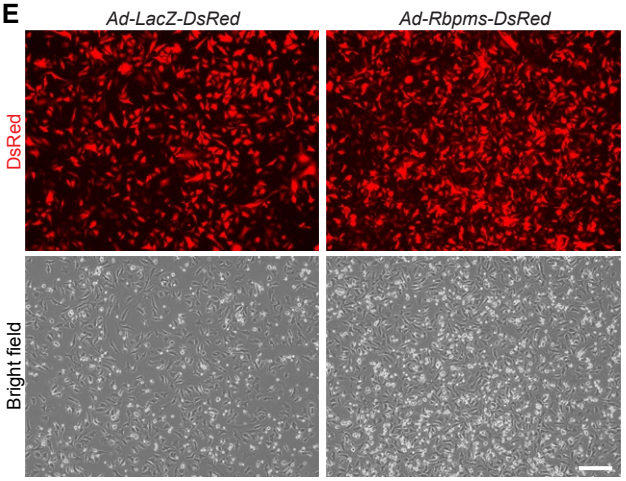

F

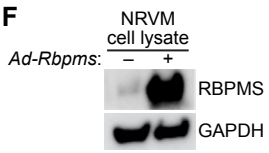

G

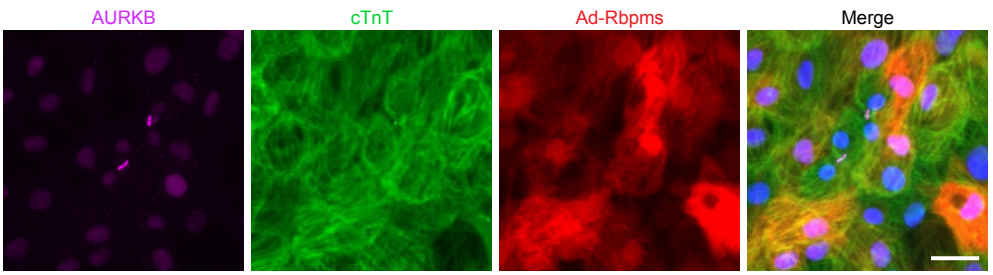

Supplemental Figure 4

Figure S4. *Rbpms* overexpression restored cytokinesis defects of *RBPMS-KO* iPSC-cardiomyocytes, Related to Figure 4.

A. Alignment of human and mouse RBPMS protein sequences. **B.** Gene structure of human *RBPMS* and knock-out strategy. Black arrow indicates the location of the sgRNA used. Boxes represent exons and UTR. Sequencing tracks demonstrate the position of the 1bp insertion in *RBPMS* exon 2 and the predicted protein sequences of translated *RBPMS* ORFs in WT and KO (clone 10) hiPSC lines. **C.** Western blot analysis showing loss of RBPMS protein expression in KO hiPSC line. GAPDH is a loading control. **D.** Immunofluorescence staining for RBPMS, cTnT and DAPI in WT and KO hiPSC-cardiomyocytes. Scale bar: 10 μm. **E.** Fluorescence and bright-field images showing infection efficiencies of *Ad-Rbpms-DsRed* and *Ad-LacZ-DsRed* in neonatal rat ventricular cardiomyocytes (NRVMs). Scale bar: 100 μm. **F.** Western blot analysis showing the overexpression of RBPMS protein in NRVMs by *Ad-Rbpms-DsRed* infection. GAPDH is a loading control. **G.** Representative immunofluorescence staining of *Ad-Rbpms* infected *RBPMS-KO* hiPSC-CMs for AURKB, and cTnT. Scale bar: 25 μm.

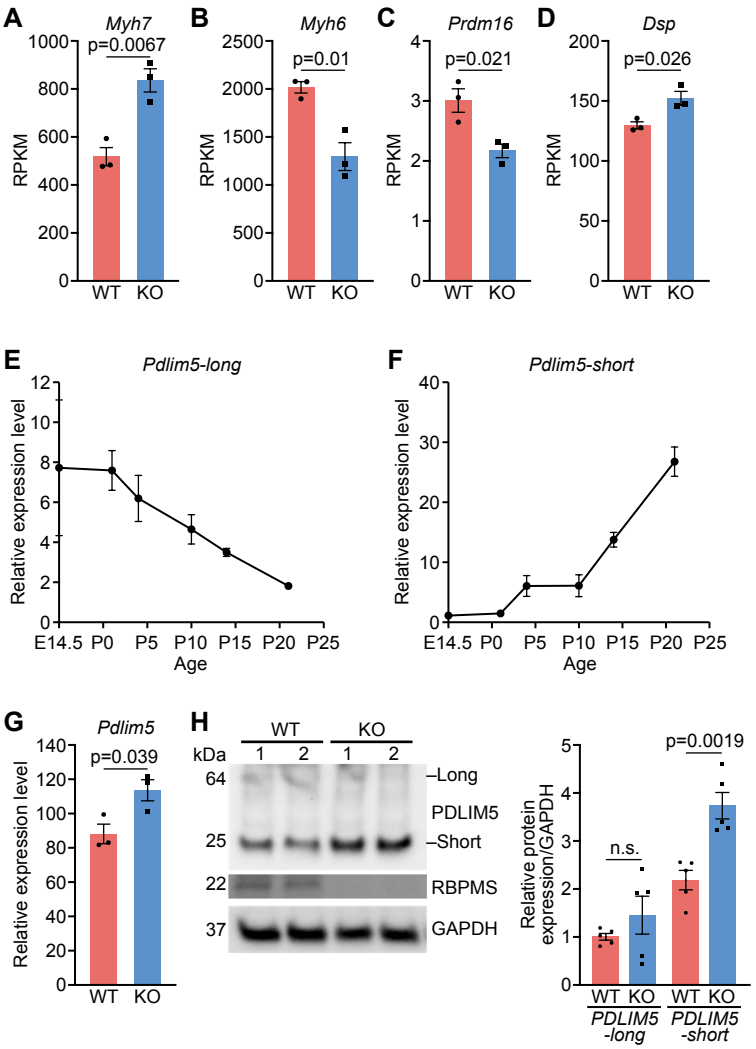

Supplemental Figure 5

Figure S5. *Pdlim5* expression in WT and *Rbpms* KO mouse hearts, Related to Figure 5.

A-D. Expression levels of *Myh7*, *Myh6*, *Prdm16* and *Dsp* transcripts in P1 WT and KO hearts, measured by bulk RNA-seq analysis (n = 3 for WT and KO). **E, F.** Relative expression levels of *Pdlim5*-long and short isoforms in C57BL/6 mouse hearts at different developmental time point measured by qRT-PCR (n = 4-6 for each time point). **G.** Relative expression level of *Pdlim5* in P1 WT and KO hearts, measured by bulk RNA-seq analysis (n = 3 for WT and KO). **H.** Western blot analysis showing the expression of PDLIM5 long and short isoform proteins in P1 WT and KO heart ventricles (Left). GAPDH is a loading control. Densitometry quantification of PDLIM5 long and short isoform proteins from western blots (Right). The intensity of each protein was normalized to GAPDH intensity (n = 5 for WT and KO). All data are presented as mean ± SEM.

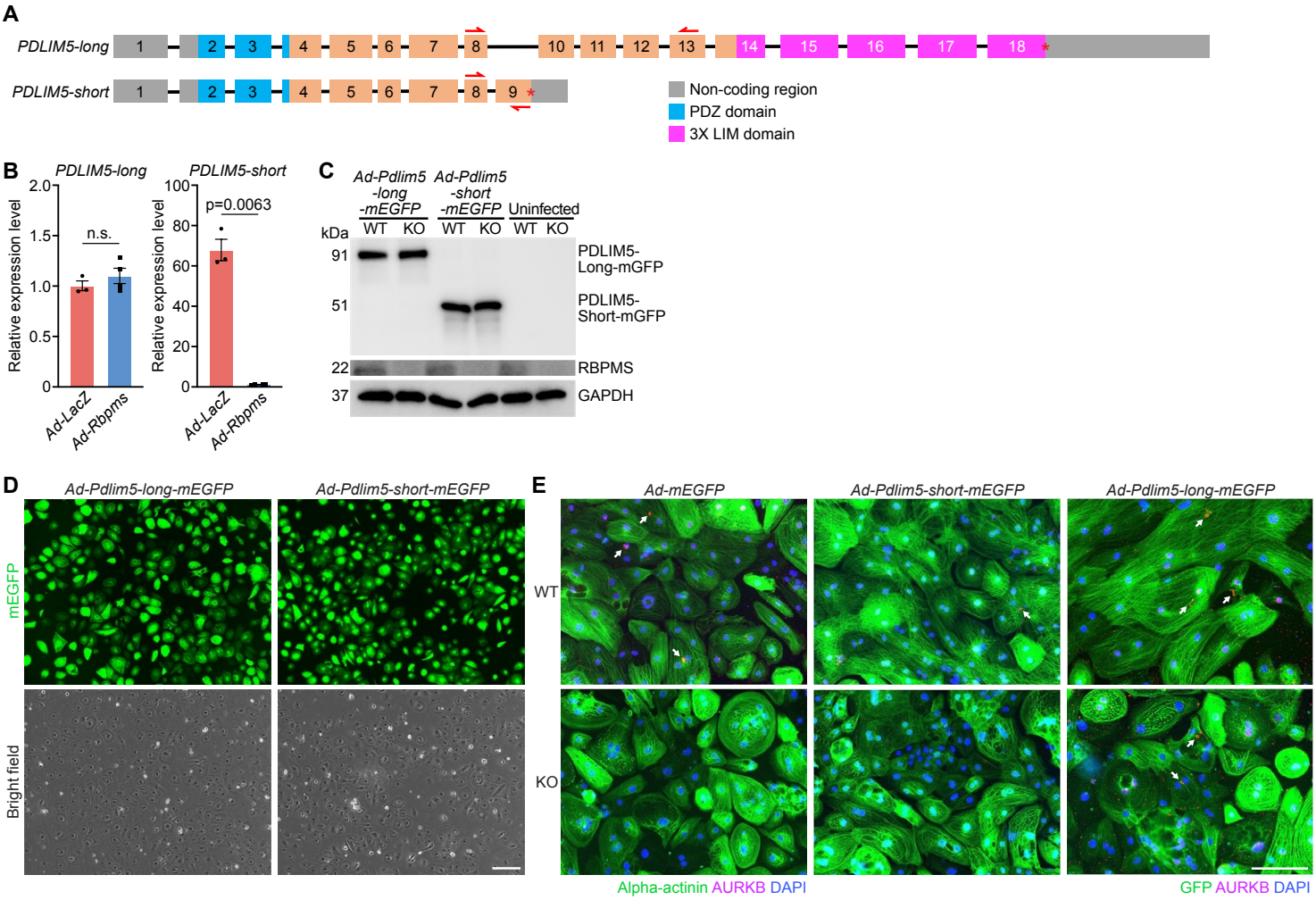

Supplemental Figure 6

Figure S6. Assessment of *Pdlim5*-long and short isoforms on cardiomyocyte cytokinesis, Related to Figure 6.

A. Schematic of human *PDLIM5* long and short isoform gene structures. Boxes represent exons, different functional domains are labelled with different colors. Horizontal red arrows indicate the locations of different qRT-PCR primers for determining long and short isoforms expression. **B.** qRT-PCR quantification of the relative expression levels of *PDLIM5* long and short isoforms in KO hiPSC-cardiomyocytes infected with *Ad-LacZ* and *Ad-Rbpms* (n = 3 for WT groups, and 4 for KO groups, n.s., not significant). **C.** Western blot analysis showing the overexpression of *Pdlim5* long and short isoforms in WT and KO hiPSC-cardiomyocytes. GAPDH is a loading control. **D.** Fluorescence and bright-field images showing the infection efficiencies of *Ad-Pdlim5-long-mEGFP* and *Ad-Pdlim5-short-mEGFP* in hiPSC-cardiomyocytes. Scale bar: 100 μm. **E.** Immunofluorescence staining for AURKB, alpha-actinin, and DAPI. White arrows indicate AURKB-positive midbodies between nuclei. Scale bar: 200 μm. All data are presented as mean ± SEM.

	+/+ (n=4)	+/- (n=5)	P-value	Significant
LVAW;d, mm	0.80 ± 0.088	0.70 ± 0.029	0.039	✔
LVAW;s, mm	1.39 ± 0.050	1.33 ± 0.065	0.17	
LVID;d, mm	2.96 ± 0.17	3.18 ± 0.21	0.14	
LVID;s, mm	1.54 ± 0.16	1.79 ± 0.16	0.053	
LVPW;d, mm	0.92 ± 0.071	0.86 ± 0.11	0.35	
LVPW;s, mm	1.52 ± 0.11	1.44 ± 0.099	0.30	
FS, %	47.88 ± 2.81	43.85 ± 2.05	0.041	✔
LVEDV, µm	33.95 ± 4.72	40.60 ± 6.71	0.14	
LVESV, µm	6.63 ± 1.68	9.66 ± 2.17	0.056	
EF, %	80.67 ± 2.86	76.35 ± 2.38	0.043	✔
HR, bpm	728.11 ± 21.63	723.60 ± 46.97	0.87	

Supplemental Table 1

Supplemental Tables

Supplemental Table 1. Echocardiography parameters of WT and *Rbpms* het mice. Related to Figure 1.

qRT-PCR primers	Sequence (5′-3′)
Mouse-Pdlim5-long/short-F	TGACAGAATCTGAAAATGACAA
Mouse-Pdlim5-short-R	CTGTACATTAAGAGCACGTGCT
Mouse-Pdlim5-long-R	TGGTTTGGACGCTGCCAGCTAGG
Alternative mouse-Pdlim5-short-F	CCGTCCAGAAGAAAACACAC
Alternative mouse-Pdlim5-short-R	TGTGATAAAACTCCGTGTTGC
Alternative mouse-Pdlim5-long-F	TCTGGGATACACTTGGCATGAT
Alternative mouse-Pdlim5-long-R	GCCCTTCCAAACTTTCACAACA
Mouse-Gapdh-F	AGGTCGGTGTGAACGGATTTG
Mouse-Gapdh-R	TGTAGACCATGTAGTTGAGGTCA
Mouse-18S-F	ACCGCAGCTAGGAATGGA
Mouse-18S-R	GCCTCAGTTCCGAAAACCA
Human-PDLIM5-long/short-F	AAAGAATCTGAAGCCGATAATA
Human-PDLIM5-short-R	GTTAAGAGCACGTGCTGAAACTTC
Human-PDLIM5-long-R	AACCCCTGGTCTGCCAGAGGTTGG
Human-GAPDH-F	GTCTCCTCTGACTTCAACAGCG
Human-GAPDH-R	ACCACCCTGTTGCTGTAGCCAA

Primers for splicing event verification	Sequence (5′-3′)
Ryr2-SE-F	AATGTTCCCCCGGACCTGTCTATCTG
Ryr2-SE-R	TGTCCGGTGGCCTCCACCTTGAGCA
Tpm2-SE6-F	AGGAGCTTCGAACCATGGAC
Tpm2-SE-R	AGCTTCTCCTCCAGAAGTTTG
Camk2g-MXE-F	ACAAGAAGTCAGATGGCGGTG
Camk2g-MXE-R	CTTGATCCCATCTGTAGCATTA
Actn1-MXE-F	GCCTCTTTCAACCACTTTGACCGG
Actn1-MXE-R	GATTCGGGCAAACTCTGCCTCTCC
Asph-SE-F	ATGTGGATGATGCCAAAGTTTT
Asph-SE-R	TCTCCTGCCAGCCCATCTGCTTC
Cald1-SE-F	GAAGAACAGCTATCAGGATGCT
Cald1-SE-R	GCACCTTCAGCTTCCTTGTCCCC
Nexn-SE-F	GAATTAGCAAAAAGAGCGGAGCAG
Nexn-SE-R	AAATCTCTGGGGAATCATCATCTAA
Tnnt2-MXE-F	AGGTGGTGGAGGAGTACGAGGA
Tnnt2-MXE-R	CCTCCTCCACTGCCTCCTCTTGCT
Ttn-SE-F	CAGTGGTACCCAAAGTCATAGTTGCCAC
Ttn-SE-R	CACAGCAGCTACAACTGTTGCCAC
Nebl-SE-F	GCTTCACTCCCGTTGTGGATGATC
Nebl-SE-R	GCATTGACCTCATGGACGACACG

Supplemental Table 2

Supplemental Table 2. Sequence information of qRT-PCR and splicing event verification primers. Related to STAR Methods sections: Quantitative Real Time PCR Analysis and Paired-end RNA-Sequencing (RNA-seq) and alternative splicing analysis.